Single-molecule diffusion measurements of H-Ras at the plasma membrane of live cells reveal microdomain localization upon activation

Piet H. M. Lommerse[1,2]**, B. Ewa Snaar-Jagalska**[2]**, Herman P. Spaink**[2]** and Thomas Schmidt**[1,*]

[1]Department of Biophysics, Leiden Institute of Physics, Leiden University, Niels Bohrweg 2, 2333 CA Leiden, The Netherlands
[2]Department of Molecular Cell Biology, Institute of Biology, Leiden University, Wassenaarseweg 64, 2333 AL Leiden, The Netherlands
*Author for correspondence (e-mail: schmidt@physics.leidenuniv.nl)

Journal of Cell Science

Summary

Recent studies show that the partitioning of the small GTPase H-Ras in different types of membrane microdomains is dependent on guanosine 5′-triphosphate (GTP)-loading of H-Ras. Detailed knowledge about the in vivo dynamics of this phenomenon is limited. In this report, the effect of the activation of H-Ras on its microdomain localization was studied by single-molecule fluorescence microscopy. Individual human H-Ras molecules fused to the enhanced yellow fluorescent protein (eYFP) were imaged in the dorsal plasma membrane of live mouse cells and their diffusion behavior was analyzed. The diffusion of a constitutively inactive (S17N) and constitutively active (G12V) mutant of H-Ras was compared. Detailed analysis revealed that for both mutants a major, fast-diffusing population and a minor, slow-diffusing population were present. The slow-diffusing fraction of the active mutant was confined to 200 nm domains, which were not observed for the inactive mutant. In line with these results we observed that the slow-diffusing fraction of wild-type H-Ras became confined to 200 nm domains upon insulin-induced activation of wild-type H-Ras. This activation-dependent localization of H-Ras to 200 nm domains, for the first time directly detected in live cells, supports the proposed relationship between H-Ras microdomain localization and activation.

Key words: H-Ras, microdomains, single-molecule diffusion, fluorescence microscopy

Introduction

Ras proteins are small GTPases that regulate cell growth, proliferation and differentiation. They are mainly localized at the plasma membrane, but also found on endosomes, the endoplasmic reticulum (ER) and the Golgi apparatus (Hancock et al., 1990; Hancock et al., 1991; Choy et al., 1999; Apolloni et al., 2000). Several isoforms of Ras: N-Ras, H-Ras and K-Ras, exist in human cells. These isoforms differ most in their 25 amino acid carboxyl-terminal region, called the hyper variable region (HVR) (Willumsen et al., 1984). The HVR contains the well-characterized membrane anchoring sequences of the Ras proteins. The minimal membrane anchor of Ras consists of the CAAX-motif, which is supplemented by one (N-Ras and K-Ras4A) or two (H-Ras) palmitoylation sites or a polybasic sequence (K-Ras4B, referred to here as K-Ras) (Hancock et al., 1990). Guanine nucleotide exchange factors (GEFs) activate Ras by facilitating GDP release and allow GTP binding by Ras (Quilliam et al., 2002). The activated, GTP-bound form of Ras can subsequently activate various effector proteins including Raf kinases, phosphatidylinositide 3-kinase (PI 3-kinase), Ral GEFs and NORE/MST1 (Ehrhardt et al., 2002). Ras signaling is turned off by GTPase activating proteins (GAPs), which stimulate the intrinsic GTPase activity of Ras (Bernards, 2003).

The different isoforms of Ras activate a variety of effectors to a different extent in cells. K-Ras, for example, is a more

potent activator of Raf-1 than H-Ras, but the latter is a more potent activator of PI 3-kinase (Yan et al., 1998; Voice et al., 1999). Interestingly, it has not been possible yet to reproduce these differences in vitro (Suire et al., 2002), raising the question of what is causing the effector specificity of Ras isoforms in cells. The notion that the membrane environment is disrupted in these in vitro experiments, combined with the fact that the major difference between H-Ras and K-Ras is found in their C-terminal, membrane-anchoring region, lead to the hypothesis that the difference in membrane anchors is involved in the observed in vivo effector specificity of Ras isoforms.

A possible mechanism by which the different Ras membrane anchors can cause the effector specificity is provided by the existence of membrane microdomains into which the anchors partition to a different extent. These microdomains include caveolae (van Deurs et al., 2003) and lipid rafts. The latter are cholesterol-dependent, liquid-ordered domains, enriched in saturated acyl chain lipids (van Meer and Simons, 1988; Simons and Ikonen, 1997). The biochemical equivalent of the in vivo lipid raft is called the detergent resistant membrane (DRM) fraction (Brown and Rose, 1992). It was discovered that Ras isoforms partition in this DRM fraction to a different extent, where H-Ras has the highest affinity and K-Ras the lowest affinity (Prior et al., 2001; Niv et al., 2002). These biochemical results were confirmed by a recent electron microscopy (EM) study, which showed the H-Ras membrane

anchor is located in cholesterol-dependent structures with a diameter of 44 nm (Prior et al., 2003), whereas the K-Ras membrane anchor is located in cholesterol-independent structures with a diameter of 32 nm.

Evidence for a relation between microdomain localization and activation of H-Ras was provided by biochemical and microscopy studies (Prior et al., 2001; Parmryd et al., 2003; Niv et al., 2002), which indicate that lipid rafts are likely to be involved in separating H-Ras molecules depending on GTP loading. GDP-loaded, inactive H-Ras was found to be partially localized in 44 nm lipid rafts, but active, GTP-loaded H-Ras was essentially absent from these structures. Instead GTP-loaded, active H-Ras seems to be localized in small (40-50 nm diameter) cholesterol-independent microdomains, recently observed by EM (Prior et al., 2003). The association of active H-Ras with these domains is stabilized by galectin-1, a lectin implicated in human tumors (Elad-Sfadia et al., 2002). The results obtained by EM (Prior et al., 2003) agree with a fluorescence recovery after photobleaching (FRAP) study of GFP-H-Ras, which showed that the lateral mobility of constitutive active GFP-H-Ras(V12) increased with the expression level in a saturable manner, suggesting a dynamic association with mobile, saturable sites or domains (Niv et al., 2002). In the same FRAP study it was shown that the mobility of GDP-loaded GFP-H-Ras(wt) did not increase with the expression level, but rather upon cholesterol depletion, indicating an association with lipid rafts. The results of these FRAP and EM studies were recently extended and combined into a model for H-Ras activation and microdomain localization (Rotblat et al., 2004).

The relationship between Ras mobility and activation was further investigated in living cells using single-molecule fluorescence resonance energy transfer (FRET) (Murakoshi et al., 2004). The study showed that the mobility of H-Ras and K-Ras is severely reduced upon activation of Ras, presumably by binding of activated Ras to specific scaffolding proteins. According to the model put forward, this binding would initiate the cooperative formation of transient signaling complexes that contain Ras effector and Ras deactivating molecules. Trapping of these signaling complexes by the actin-based membrane skeleton (Fujiwara et al., 2002) would result in the strong decrease of mobility that was observed for activated Ras.

Taken together, the results of previous studies indicate a dynamic and activation-dependent association of Ras isoforms with different types of membrane domains, and in addition, the formation of signaling complexes upon Ras activation. To what extent the membrane domains and signaling complexes are related remains unclear, but they are presumably responsible for the observed differences in effector activation in vivo.

To obtain more detailed insight into the relationship between microdomain localization and activation of H-Ras in vivo, we employed single-molecule fluorescence microscopy. The high positional accuracy (~35 nm) and temporal resolution (milliseconds) of this technique offer the possibility to directly observe even small, transient domains and subpopulations in vivo. Wild-type H-Ras, a constitutive active mutant (G12V) (Seeburg et al., 1984) and an constitutive inactive mutant (S17N) (Feig and Cooper, 1988; Farnsworth and Feig, 1991) were fused to the enhanced yellow fluorescent protein (eYFP) and expressed

at a low level in 3T3-A14 mouse fibroblast cells. Analysis of single-molecule trajectories showed that all the eYFP-H-Ras constructs had a large fast-diffusing fraction and a smaller, slow-diffusing fraction. Both fractions were diffusing freely for both the inactive H-Ras mutant (S17N) and GDP-loaded wild-type H-Ras. In contrast, for the active H-Ras mutant (G12V) and GTP-loaded wild-type H-Ras, the slow-diffusing fraction was confined to ~200 nm-sized domains. The potential role of these newly discovered Ras-activation-dependent 200 nm domains will be discussed in the context of the existing models for Ras activation, diffusion and microdomains.

Materials and Methods

Plasmids

pcDNA3.1-eYFP was made by cutting the eYFP coding sequence out of peYFP (BD Biosciences, Alphen aan den Rijn, The Netherlands) using *Bam*HI and *Not*I and ligated into *Bam*HI-*Not*I cut pcDNA3.1 (Invitrogen, Breda, The Netherlands). Pmt2 vectors containing the human H-Ras(wt), H-Ras(V12) and H-Ras(N17) coding sequences were subjected to PCR. The primers introduced a *Bsr*GI site at the 5′ end of the H-Ras coding sequence and an *Xho*I site at the 3′ end. After PCR, the resulting products were purified using a QIAquick PCR Purification Kit (Qiagen, Hilden, Germany), A-tailed using Taq polymerase, size-checked on agarose gel and ligated into the pGEM-T easy vector (Promega Benelux BV, Leiden, The Netherlands). The H-Ras coding sequences were cut out using *Bsr*GI-*Xho*I and ligated in frame into *Bsr*GI-*Xho*I-digested pcDNA3.1-eYFP. The integrity of the resulting eYFP-H-Ras reading frames was checked by sequence analysis.

Cell culture and transfection

For all experiments a mouse fibroblast cell line stably expressing the human insulin receptor (3T3-A14) was used (Burgering et al., 1991). Cells were cultured in DMEM medium supplemented with streptomycin (100 μg/ml), penicillin (100 U/ml) and 10% bovine serum in a 7% CO_2 humidified atmosphere at 37°C (95% humidity). Cells were used for 12-14 passages and were transferred every 4 days. For microscopy purposes the cells were cultured on no. 1 glass slides (Fisher Scientific, 's-Hertogenbosch, The Netherlands). Cell cultures at a confluency of 20-30% were used for transfection with 1.0 μg DNA and 3 μl FuGENE 6 (Roche Molecular Biochemicals, Indianapolis, USA) per glass slide. The transfection efficiency, as determined by fluorescence microscopy 48 hours after transfection, was about 30%.

Detection and quantification of GTP loading of eYFP-H-Ras

3T3-A14 cells (Burgering et al., 1991) cultured in 60 mm dishes were transfected with eYFP-H-Ras fusion constructs 48 hours before the GTP-loading assay. The transfection efficiency, as determined after 48 hours by fluorescence microscopy, was 30% for all constructs. The cells were serum-starved by replacement of the culture medium with DMEM/0.5%BSA 18 hours before the GTP-loading assay. Activation of H-Ras was achieved by a 5-minute incubation with 10 μg/ml insulin (Sigma-Aldrich Chemie B.V., Zwijndrecht, The Netherlands). After stimulation, the cells were quickly washed with ice-cold phosphate-buffered saline (PBS: 150 mM NaCl, 10 mM Na_2HPO_4/NaH_2PO_4, pH 7.4) and lysed in 0.5 ml ice-cold lysis buffer [25 mM Hepes, pH 7.5, 150 mM NaCl, 1% Igepal CA-630, 10 mM $MgCl_2$, 1 mM EDTA, 2% glycerol, 1 mM sodium orthovanadate, 25 mM sodium fluoride, protease inhibitor cocktail (complete Mini EDTA free; Roche Diagnostics, Basel, Switzerland)]. The cell lysate was diluted to a total cell protein concentration of 1 μg/μl, as determined by the Bradford assay

(Bradford, 1976). Ras-GTP of 400 µg of total cell lysate was precipitated by addition of 7.5 µg Raf-1 Ras binding domain (RBD) agarose beads (Upstate Ltd, UK), whereas 50 µg of total cell lysate was used for determination of eYFP-Ras level. After SDS-PAGE, eYFP-Ras (molecular mass of ~50 kDa) was identified by western blotting using anti-Ras (1:2000; Anti-Ras, clone RAS10, Upstate Ltd, UK) followed by goat anti-mouse HRP-conjugated IgG 1:5000 (supplied with ECL kit, NA931) and chemiluminescence detection (ECL kit; Amersham Biosciences Europe GmbH, Roosendaal, The Netherlands).

Activation of mitogen-activated protein kinase (MAPK) cascade

To show that the fusion of eYFP to H-Ras(wt) did not influence the downstream signaling, the phosphorylation of the extracellular-signal-regulated kinase 1 (ERK1, 44 kDa) and ERK2 (42 kDa) was tested. Activation of Ras by insulin, preparation of the cell lysates, SDS-PAGE and blotting were performed as described in the previous section. ERK1 and ERK2 were detected using an anti-ERK antibody (1:3000; Santa Cruz, CA, USA). The phosphorylation of the amino acids Thr202/Tyr204 of ERK1 and ERK2 was specifically detected using a phospho-p44/42-MAPK antibody (1:1000; Cell Signaling Technology, Beverly, MA, USA). Immunoreactive bands were visualized by incubation with goat anti-rabbit HRP-conjugated IgG 1:10000 (supplied with ECL kit, NA934) and chemiluminescence detection (ECL-kit, Amersham Biosciences Europe GmbH, Roosendaal, The Netherlands).

Single-molecule fluorescence microscopy

The experimental arrangement for single-molecule imaging has been described in detail previously (Schmidt et al., 1995; Lommerse et al., 2004). Briefly, 3T3-A14 cells adherent to glass slides were mounted onto the microscope and kept in PBS at 37°C. For the observation of the mobility of individual eYFP-H-Ras molecules the focus of the microscope was set to the dorsal plasma membrane of individual cells (depth of focus ~1 µm). Measuring at the dorsal plasma membrane eliminates potential effects of the cellular attachment to the glass-slide on the diffusion. The density of fluorescent proteins on the plasma membrane of selected transfected cells (6-7 days post-transfection) was less than 1 µm^{-2}, which permitted imaging and tracking of individual fluorophores and ensured that dimerization of fluorescent proteins (Zacharias et al., 2002) was minimized. Fluorescence images were taken consecutively with up to 1000 images per sequence. For the wild-type H-Ras, sequences of the same cell were recorded before and after the addition of insulin (final concentration 10 µg/ml) to the cell bath. After addition the insulin was continuously present. Visual inspection of the cells at the end of the experiments (20 minutes after addition of insulin) revealed no observable changes in cell morphology.

Tracking of molecules and analysis of square displacements

By connectivity analysis between consecutive images the two-dimensional trajectories of individual molecules in the plane of focus were reconstructed (Schmidt et al., 1995). These trajectories were up to nine steps in length, mainly limited by the blinking and photobleaching of the fluorophore (Harms et al., 2001). To compensate for the limited length of individual trajectories, multiple data sets, each consisting of hundreds of trajectories from 6-23 cells per experimental condition, were analyzed. In addition, data sets were acquired with different times between consecutive images (timelag, t_{lag}), varying from 5 to 60 milliseconds (ms). The trajectories were analyzed in terms of square displacement (r^2), following a method developed previously (Schütz et al., 1997). Briefly, cumulative probability distributions $P(r^2, t_{lag})$ were constructed for every timelag by counting the number of square displacements with values $\leq r^2$ and subsequent normalization by the total number of data points ($n>60$). These cumulative probability distributions of square displacements were fitted to models that are described in the next section.

Models to analyze square displacement distributions

The lateral diffusion of Brownian particles in a medium characterized by a diffusion coefficient D is described by the cumulative distribution function of the square displacements, r^2 (Anderson et al., 1992; Almeida and Vaz, 1995):

$$P(r^2, t_{lag}) = 1 - \exp\left(-\frac{r^2}{r_0^2(t_{lag})}\right). \quad (1)$$

$P(r^2, t_{lag})$ describes the probability that the Brownian particle starting at the origin will be found within a circle of radius r at time t_{lag}. It is characterized by the mean-square displacement of $r_0^2(t_{lag}) = 4Dt_{lag}$ (Anderson et al., 1992). In a previous study on the H-Ras membrane anchor (Lommerse et al., 2004) it was shown that there are two types of mobility for these molecules, one with high and one with low mobility, characterized by diffusion coefficient D_1 and D_2, and relative fractions α and $(1-\alpha)$, respectively. In this case, the cumulative probability distribution function for the square displacements, r^2, becomes (Schütz et al., 1997):

$$P(r^2, t_{lag}) =$$

$$1 - \left[\alpha \cdot \exp\left(-\frac{r^2}{r_1^2(t_{lag})}\right) + (1-\alpha) \cdot \exp\left(-\frac{r^2}{r_2^2(t_{lag})}\right)\right], \quad (2)$$

with mean-square displacements of $r_i^2(t_{lag}) = 4D_i t_{lag}$, i=1, 2.

This analysis resulted in a parameter set consisting of the fraction of fast-diffusing molecules (α), the mean square displacement corresponding to the fast fraction (r_1^2), and the mean square displacement of the slow-diffusing fraction (r_2^2) of molecules, for each timelag, t_{lag}. This approach of fitting the probability distributions leads to a robust estimate of the mean square displacements r_1^2 and r_2^2 even when the mobility is not purely random.

Mobility analysis

By plotting r_1^2 and r_2^2 (obtained from the fits according to Eqn 2) versus t_{lag}, the diffusion behavior of the respective populations of molecules is revealed. These (r_i^2, t_{lag}) datasets were fitted either by a free diffusion model ($r_i^2 = 4D_i t_{lag}$) or by a confined diffusion model. The confined diffusion model assumes that diffusion is free within a square of side length L, surrounded by an impermeable, reflecting barrier. In such a model the mean square displacement depends on L and the initial diffusion coefficient D_0, and varies with t_{lag} as (Kusumi et al., 1993):

$$r_i^2(t_{lag}) = \frac{L^2}{3} \cdot \left[1 - \exp\left(\frac{-12D_0 t_{lag}}{L^2}\right)\right]. \quad (3)$$

Both the confined diffusion model and the free diffusion model were fitted to (r_2^2, t_{lag}) data (see Table 1). The best-fitting model was used for further analysis. The limited positional accuracy of our measurements (~35 nm) resulted in a constant offset in r_i^2 of $4 \times (35$ nm)$^2 = 0.49 \times 10^{-2}$ µm^2 in all (r_i^2, t_{lag}) plots (Schütz et al., 1997). From this positional accuracy, we estimate that domains with a surface area of twice the positional accuracy offset (corresponding to a domain size (L) of about 120 nm) represent the smallest domains that could be observed directly in this study.

Results

Fusion of eYFP to H-Ras does not affect its localization and signaling

To study the effect of H-Ras activation on microdomain localization, a constitutively inactive mutant, H-Ras(N17), a constitutively active mutant, H-Ras(V12), and wild-type H-Ras, H-Ras(wt) were fused to the yellow fluorescent protein (eYFP). The localization of these fluorescent fusion proteins was verified by confocal microscopy in transiently transfected HEK293 and 3T3-A14 cells (Fig. 1A). All eYFP-H-Ras fusion proteins showed clear plasma membrane localization, indicating that membrane targeting was not impaired.

To test the functionality of the eYFP-H-Ras fusion proteins, 3T3-A14 cells transiently transfected with the different eYFP-H-Ras constructs were stimulated with insulin. Ras binding domain (RBD) of Raf-1 coupled to agarose beads was used to specifically recognize active, GTP-bound Ras and pull-down Ras-GTP from the cell lysate. Subsequent immunoblotting revealed that the wild-type eYFP-H-Ras fusion shifted to a GTP-bound state upon stimulation (Fig. 1B). Quantification of the 50 kDa eYFP-H-Ras(wt) band before and after stimulation, revealed a 78% increase in pulled-down GTP-loaded H-Ras(wt) after a 5-minute insulin stimulation. As expected, the constitutively active mutant, eYFP-H-Ras(V12), was in a GTP-bound state irrespective of stimulation, whereas the inactive mutant, eYFP-HRas(N17) did not show any significant GTP-loading upon stimulation (Fig. 1B).

Activation of H-Ras(wt) by insulin is known to lead to the phosphorylation of the MAP kinases ERK1/2, which is correlated with their activation (Sturgill et al., 1988; Payne et al., 1991; Cowley et al., 1994). The fusion of eYFP to H-Ras(wt) did not influence the insulin-induced ERK1/2 phosphorylation, as visualized by a specific dual-phosphorylation antibody (Fig. 1C). In conclusion, fusion of eYFP to the N terminus of the H-Ras proteins did not affect either their localization or the downstream signaling capabilities that we tested.

Individual eYFP-H-Ras molecules observed on the dorsal plasma membrane of live 3T3-A14 cells

The observation of individual eYFP-H-Ras molecules on the dorsal plasma membrane of live 3T3-A14 cells required low densities of these molecules on the plasma membrane (<1 μm^{-2}). This was achieved by using cells 6-7 days after transfection. At the dorsal membrane (30-60 μm^2) diffraction-limited, fluorescent signals were observed (Fig. 2A). These signals had intensities comparable to values obtained previously for single, monomeric eYFP molecules (Harms et al., 2001; Lommerse et al., 2004) In addition, the signals showed single-step photobleaching behavior (Fig. 2B), indicative for the observation of individual fluorophores. Analysis of the fluorescence signals of 3028 individual eYFP-H-Ras(wt) molecules at the dorsal membrane of 3T3-A14 cells in unstimulated conditions (Fig. 2C), yielded an intensity distribution characteristic for monomeric eYFP. The signal-to-background noise ratio of about 20 in the images enabled us to determine the position of individual eYFP molecules with an accuracy of ~35 nm (Schmidt et al., 1996). Subsequent tracking of these single-molecule signals through successive images produced trajectories of diffusing molecules (Fig. 2D). Several thousands (>3000) of such

Fig. 1. (A) Images of the localization of eYFP-H-Ras in transiently transfected HEK293 cells. Confocal images of HEK293 cells transiently expressing eYFP-H-Ras(N17), eYFP-H-Ras(V12) and eYFP-H-Ras(wt). Images were taken 48 hours after transfection. Fusions between eYFP and the wild-type H-Ras as well as both mutants of H-Ras showed clear plasma membrane localization, indicating that membrane targeting was not impaired by the eYFP fusion to H-Ras. Scale bar: 10 μm. (B) Insulin-induced GTP loading of eYFP-H-Ras(wt). Active Ras was specifically pulled-down in an RBD assay, separated on a PAA-gel, blotted and detected by anti-Ras antibody (see Materials and Methods). 3T3-A14 cells were transiently transfected with Ras membrane anchor (10 C-terminal amino acids) fused to eYFP (mt), eYFP-H-Ras(wt), eYFP-H-Ras(V12), or eYFP-H-Ras(N17). Results are shown for unstimulated (–) and 5-minute insulin-stimulated (+) conditions. A clear increase of GTP loading was observed for wild-type eYFP-H-Ras (~50 kDa) after stimulation, as well as for endogenous Ras (~21 kDa). (C) Activation of extracellular regulated kinases (ERKs) in the presence of eYFP-H-Ras(wt). Results are shown for unstimulated (–) and 5-minute insulin-stimulated (+) conditions. To show that the fusion of eYFP to H-Ras(wt) did impair downstream signaling, the phosphorylation of the MAPK-kinases ERK1 (44 kDa) and ERK2 (42 kDa) was tested. Activation of Ras by insulin, preparation of the cell lysates, SDS-PAGE and blotting were performed as described in Materials and Methods. The left part of the immunoblot (anti-ERK) shows total ERK1 and ERK2 in cell lysates of 3T3-A14 cells transiently transfected with eYFP-H-Ras(wt). The phosphorylation of ERK1 and ERK2 upon insulin addition is shown on the right (anti-ERK-P). The phosphorylation of the amino acids Thr202 and Tyr204 of ERK1 and ERK2 was specifically detected using a phospho-p44/42-MAPK antibody (Cell Signaling Technology, Beverly, MA, USA).
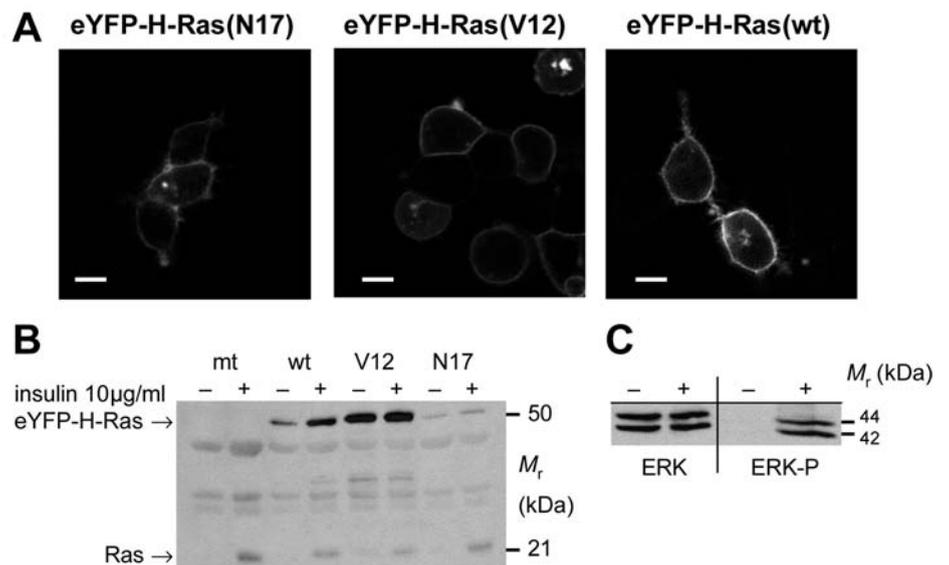
trajectories were obtained for each of the H-Ras constructs studied.

Square-displacement distribution analysis of inactive and active H-Ras revealed differences in mobility

For each timelag the distribution of square displacements was analyzed by plotting the square displacement (r^2) values against the cumulative probability (see Materials and Methods). In Fig. 3A, square displacement distributions of the active (V12) and the inactive mutant (N17) are compared for a timelag of 50 ms. This comparison revealed that the eYFP-H-Ras(V12) square displacement distribution was shifted to lower square displacement values with respect to eYFP-H-Ras(N17). A similar, though less strong, shift was observed for eYFP-H-Ras(wt) when unstimulated and 5-minute-insulin-stimulated square displacement distributions are compared (Fig. 3D).
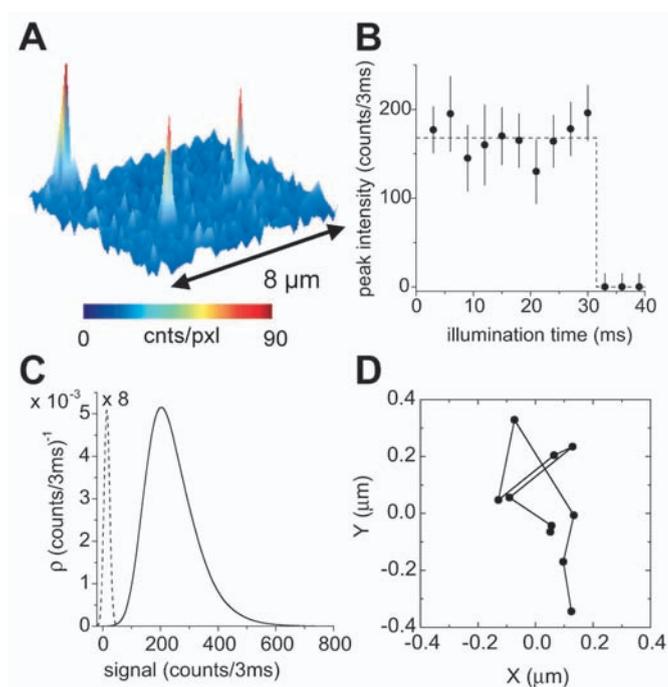

Fig. 2. Tracking individual eYFP-H-Ras(wt) molecules in the plasma membrane of live cells. (A) Image showing three single-molecule signals of eYFP-H-Ras(wt) molecules at the dorsal plasma membrane of a 3T3-A14 cell. The image was taken using 514 nm illumination for 3 mseconds at 2 kW/cm². Scale bar: 1 μm. (B) Example of a single-step photobleaching event of an individual eYFP-H-Ras(wt) molecule. (C) Probability density of the single molecule fluorescence intensity of eYFP-H-Ras(wt). Analysis of the signals of 3028 individual eYFP-H-Ras(wt) molecules at the dorsal plasma membrane of 3T3-A14 cells (solid line) in unstimulated conditions. The probability density of the fluorescence intensity is nearly Gaussian-shaped with a maximum of 204 counts/3 milliseconds. Statistics of the background signal (dashed line) is shown for comparison. The backgound signal had a maximum at 14 counts/3 milliseconds and a width of σ=10 counts/3 milliseconds. These values translate into a signal to background noise ratio of 20. (D) Trajectory of an eYFP-H-Ras(wt) molecule diffusing in the dorsal plasma membrane of a 3T3-A14 cell. The time between subsequent steps was 10 milliseconds.

To quantify these effects, the square displacement distributions were fitted to a one-component model (Eqn 1), which assumes one population of mobile molecules to be present. A fit of the one-component model to the data resulted in the dashed lines in Fig. 3B,C,E and F, which clearly show that this model fails to describe the data. A two-component model (Eqn 2), which assumes two populations of mobile molecules to be present, resulted in a satisfactory description of the data (solid lines in Fig. 3B,C,E,F). Each fit to this two-component model resulted in a set of three parameters: a fraction of fast-diffusing molecules (α), a mean square displacement of this fast fraction (r_1^2) and a mean square displacement of the slow-diffusing fraction (r_2^2) of molecules.

For eYFP-H-Ras(N17) (Fig. 3B) values of 0.87±0.08, 0.19±0.02 μm² and 0.022±0.020 μm² were obtained for α, r_1^2 and r_2^2, respectively. A fit of the comparable eYFP-H-Ras(V12) dataset (Fig. 3C), resulted in α=0.53±0.15, r_1^2=0.14±0.05 μm² and r_2^2=0.018±0.007 μm². The smaller fraction of fast-diffusing molecules (α) observed for eYFP-H-Ras(V12) compared to eYFP-H-Ras(N17) is in agreement with the shift observed in Fig. 3A. The two-component fit of eYFP-H-Ras(wt) data before insulin addition (Fig. 3E) resulted in α=0.67±0.11, r_1^2=0.33±0.07 μm² and r_2^2=0.029±0.016 μm², whereas α=0.57±0.10, r_1^2=0.25±0.07 μm² and r_2^2=0.017±0.007 μm² were obtained for the 5-minute-insulin-stimulated eYFP-H-Ras(wt) (Fig. 3F).

Diffusion analysis of eYFP-H-Ras(N17) and eYFP-H-Ras(V12) showed activation dependent mobility and domain localization

To obtain insight into the diffusion behavior, square displacement data (see Fig. 3) were obtained for different timelags (5-50 ms) and fitted to the two-component model (Eqn 2). When the values of α, r_1^2 and r_2^2 obtained from these fits were plotted versus the timelag, the diffusion behavior of the respective fast- and slow-diffusing population, and their relative sizes were revealed. The results are summarized in Fig. 4A-C and Fig. 4D-F for the inactive N17 and the active V12 mutant, respectively (see also Table 1). One of the most obvious differences between the two mutants is the size of the fast-diffusing fraction of molecules (α). For N17 the weighted mean of this fraction was α=0.84±0.05 compared with α=0.61±0.05 for V12 over all timelags. The square displacements of the fast fraction of both mutants showed a linear increase with time (Fig. 4B,E), a signature of free diffusion. The diffusion was characterized by a diffusion coefficient of D_1=1.02±0.02 μm²/second for N17, and a 17% lower diffusion coefficient of D_1=0.85±0.04 μm²/second for V12 (solid lines Fig. 4B,E).

Mean square displacement analysis of the slow-diffusing fraction of molecules also revealed a difference between the two mutants (Fig. 4C,F). The plot of the mean square displacement of the slow-diffusing population of N17 versus time is shown in Fig. 4C. The large error bars at longer timelags are due to the small size (16%) of the slow faction (Fig. 4A), resulting in larger statistical errors. A simple free-diffusion model was used to fit the data (solid line Fig. 4C) which resulted in a diffusion coefficient, D_2=0.16±0.03 μm²/second. In contrast, the mean square displacement of the slow-diffusing
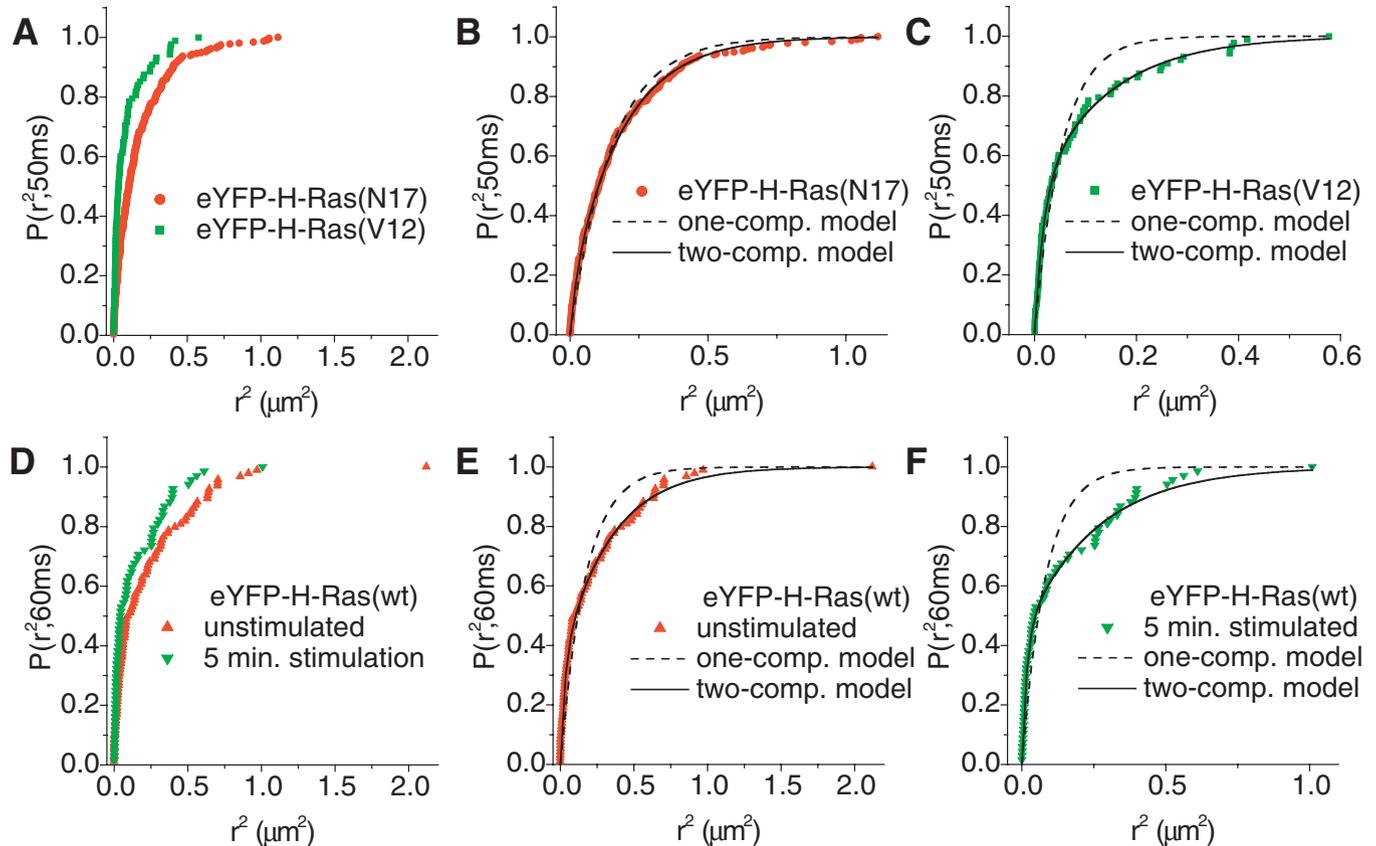
Fig. 3. Square displacement analysis of the different eYFP-H-Ras constructs. Cumulative probability, $P(r^2, t_{lag})$, plotted versus the square displacements, r^2. (A) Cumulative probability, $P(r^2, 50$ mseconds$)$ distributions of the inactive mutant eYFP-H-Ras(N17) (red dots) and the active mutant eYFP-H-Ras(V12) (green squares). These distributions were fitted to the one-component model (Eqn 1) or two-component model (Eqn 2). (B,C) Show the distributions and the results of the fits to the one-component (dashed line) and two-component (solid line) model. (D) Cumulative probability, $P(r^2, 60$ mseconds$)$ distributions of wild-type eYFP-H-Ras(wt) before (red triangles) and after 5 minutes insulin stimulation (green triangles). (E,F) The distributions and the results of the fits to the one-component (dashed line) and two-component (solid line) model. B,C,E and F clearly show that the two-component model describes the cumulative probability distributions significantly better than the one-component model. For all cumulative probability distributions of H-Ras that were obtained and analyzed in this study, the two-component model yielded significantly better fit results than the one-component model.

fraction of the V12 mutant (Fig. 4F) showed a clear leveling-off at longer timelags, indicating confinement of the diffusing molecules. A fit of the data to a confined diffusion model (Eqn 3, Materials and Methods) yielded an initial diffusion coefficient, $D_0=0.16\pm0.04$ μm^2/second and a confinement size $L=217\pm46$ nm.

In summary, the fast, free-diffusing fraction of the inactive mutant was larger and had a higher mobility than the active mutant. Moreover, the slow-diffusing fraction of the inactive mutant was freely diffusing, whereas the slow-diffusing fraction of the active mutant was confined to 200 nm-sized domains.

Activation of eYFP-H-Ras(wt) resulted in confined diffusion in small domains

To establish whether the differences in mobility and domain localization observed for the H-Ras mutants were due to the actual activation process of H-Ras, the diffusion of eYFP-H-Ras(wt) was studied from 5-60 milliseconds both before and 5, 10 and 15 minutes after insulin addition (Fig. 5, results

summarized in Table 1). The weighted mean of the fast-diffusing fraction of molecules before stimulation, $\alpha=0.75\pm0.04$ (solid line Fig. 5A), was equal to the value obtained after 5 minutes of stimulation, $\alpha=0.72\pm0.05$ (solid line, Fig. 5D). For both unstimulated and stimulated conditions the mean square displacement of the fast-diffusing fraction showed a linear increase with timelag. The fit (solid lines in Fig. 5B,E) resulted in a diffusion coefficient of $D_1=1.11\pm0.09$ μm^2/second before stimulation and $D_1=1.08\pm0.07$ μm^2/second after 5 minutes of insulin stimulation.

In contrast to the fast-diffusing fraction, the slow-diffusing fraction of molecules showed a severe change upon stimulation. Before stimulation the mean square displacement increased linearly with time (Fig. 5C), characterized by a diffusion coefficient, $D_2=0.12\pm0.03$ μm^2/second (solid line Fig. 5C). The slow-diffusing fraction showed a strongly confined behavior after 5 minutes of stimulation (Fig. 5F). This behavior was best described by a confined diffusion model (Eqn 3, solid line Fig. 5F) yielding an initial diffusion coefficient, $D_0=0.2\pm0.1$ μm^2/second and a confinement size, $L=175\pm35$ nm. These values are comparable to the ones

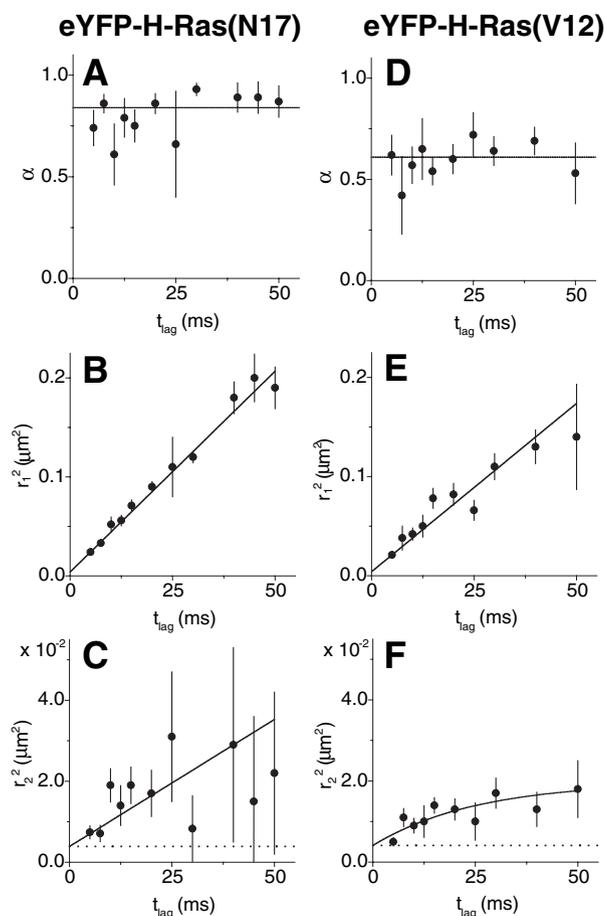## eYFP-H-Ras(N17)   eYFP-H-Ras(V12)

Fig. 4. Diffusion characteristics of eYFP-H-Ras(N17) and eYFP-H-Ras(V12). Fitting of the square displacement distributions (Fig. 3) to Eqn 2 (Materials and methods) yielded a fraction of fast-diffusing molecules, α, and corresponding characteristic mean square displacements for the fast (r_1^2) and slow (r_2^2) diffusing population of molecules for each t_{lag}. A and D, B and E, C and F show plots of α, r_1^2 and r_2^2, respectively, versus t_{lag} for both the N17 and V12 mutants. (A,D) The solid lines show the weighted mean of the fast fraction of molecules over all timelags. (B,E) Mean square displacement data of the fast-diffusing fractions were fitted according to a free diffusion model ($r_1^2=4D_1t_{lag}$, solid line). (C,F) Mean square displacement data of the slow-diffusing fractions were fitted according to a free (C) and confined (F, Eqn 3) diffusion model (solid lines). The dotted lines in C and F represent the offset due to the limited positional accuracy (see Materials and Methods), although the same offset is present in B and 4E, the dotted lines were omitted here for clarity.

obtained for the slow-diffusing fraction of the active mutant (Table 1).

Analogous analysis of α, r_1^2 and r_2^2 versus timelag was performed for 10 and 15 minutes of continuous insulin stimulation (Fig. 5G-L and Table 1). The fraction of fast-diffusing molecules did not change significantly with stimulation time, nor did the diffusion coefficient of the fast fraction. The confinement of the slow-diffusing fraction in ~200 nm domains was still present after 10 and 15 minutes of insulin stimulation (Fig. 5I,L). Hence, we have shown that activation of eYFP-H-Ras(wt) by insulin stimulation results in the confinement of the slow-diffusing fraction to 200 nm microdomains, in line with the results obtained for the H-Ras mutants (Fig. 4C,F).

Discussion

H-Ras activation results in partial localization to 200 nm domains

The main aim of this study was to investigate how the diffusion and microdomain distribution of H-Ras depend on its activation state in vivo. We fused eYFP to H-Ras(wt), H-Ras(N17) and H-Ras(V12) and used single-molecule fluorescence microscopy to study its mobility in the dorsal plasma membrane of live 3T3-A14 cells. Fig. 6A shows a schematic representation the results we obtained for the diffusion of the constitutively inactive mutant eYFP-H-Ras(N17) and of the constitutively active mutant eYFP-H-Ras(V12). A fast-diffusing population (blue in Fig. 6A) and a slow-diffusing population (green in Fig. 6A) were observed for both mutants. The slow-diffusing population of the inactive mutant showed free diffusion (green in Fig. 6A), whereas the slow-diffusing fraction of the active mutant (red in Fig. 6A) was confined to ~200 nm domains. Before insulin addition the diffusion behavior of eYFP-H-Ras(wt) resembled that of the inactive mutant (Fig. 6B). Upon activation of eYFP-H-Ras(wt) by a 5-minute insulin stimulation, a confinement of the slow-diffusing population in small ~200 nm-diameter domains (red in Fig. 6B) was observed, which prevailed for at least 10 more minutes (Table 1).

Differences and similarities with a single-molecule FRET study of H-Ras

Our data agree partially with the results of a single-molecule FRET microscopy study on H-Ras activation and mobility (Murakoshi et al., 2004). In that study YFP-H-Ras, expressed at low level in human epidermoid mouth carcinoma cells (KB

Table 1. Summary of eYFP-H-Ras diffusion characteristics

H-Ras	N17	V12	wt			
Insulin stimulation (minutes)			0	5	10	15
α	0.84±0.05	0.61±0.05	0.75±0.04	0.72±0.05	0.77±0.04	0.75±0.07
D_1 (µm²/s)	1.02±0.02	0.85±0.04	1.11±0.09	1.08±0.07	1.05±0.07	0.96±0.06
D_2 (µm²/s)	0.16±0.03	(0.10±0.01)	0.12±0.03	(0.07±0.02)	(0.08±0.02)	0.10±0.03
D_0 (µm²/s)	(0.23±0.08)	0.16±0.04	(0.12±0.04)	0.2±0.1	0.13±0.06	0.18±0.10
L (nm)	(245±77)	217±46	(731±1585)	175±35	192±70	210±67

D_1 and D_2 are the diffusion coefficients obtained for the fast- and slow-diffusing fraction, respectively, when (r_i^2, t_{lag})-plots are fitted to a free diffusion model ($r_i^2=4D_it_{lag}$). D_0 and L represent the initial diffusion coefficient and domain size obtained when the (r_2^2, t_{lag})-plots are fitted to a confined diffusion model (Eqn 3). Values in brackets result from fits to the inferior-fitting model; the values are just given for comparison.

cells), was used as a FRET donor, in combination with microinjected BodipyTR-GTP as a FRET-acceptor. The motion of individual molecules was observed at the basal membrane using total internal reflection (TIR) microscopy. Before EGF addition, analysis of the mean square displacement (MSD) in a time window of 200 milliseconds revealed that about 9% of the H-Ras molecules were immobile. Of the remaining mobile H-Ras molecules, more than 90% exhibited rapid free diffusion. EGF-induced Ras activation resulted in a severely reduced mobility of H-Ras: about half of the activated H-Ras molecules were immobile and the remaining mobile H-Ras molecules were slowed down by a factor of three to four.

A detailed comparison of the results of this FRET study to our data (Fig. 6, Table 1), reveals some differences. In the current study non-activated H-Ras(wt) shows a major (75%)

fast-diffusing fraction and a minor (25%) slow-diffusing fraction (Table 1). The FRET study on the other hand, finds a large (91%) mobile and small (9%) immobile fraction for non-activated H-Ras(wt). In addition, we observed the localization of about 25% of H-Ras(wt) to 200-nm domains upon activation, whereas the FRET study just showed a slow-down and partial immobilization of activated H-Ras. These differences are not too surprising considering that the two studies use different cells types (3T3 versus KB), measured mobility at different membranes (dorsal versus basal) and timescales (60 milliseconds versus 200 milliseconds). All of these factors probably affect the exact, quantitative outcome of the H-Ras diffusion. The molecules trapped in the 200 nm domains, detected in our study on a 60 millisecond timescale, show MSD values close to or below 0.018 μm^2 (Fig. 4F and Fig. 5F), a value below which molecules were classified as
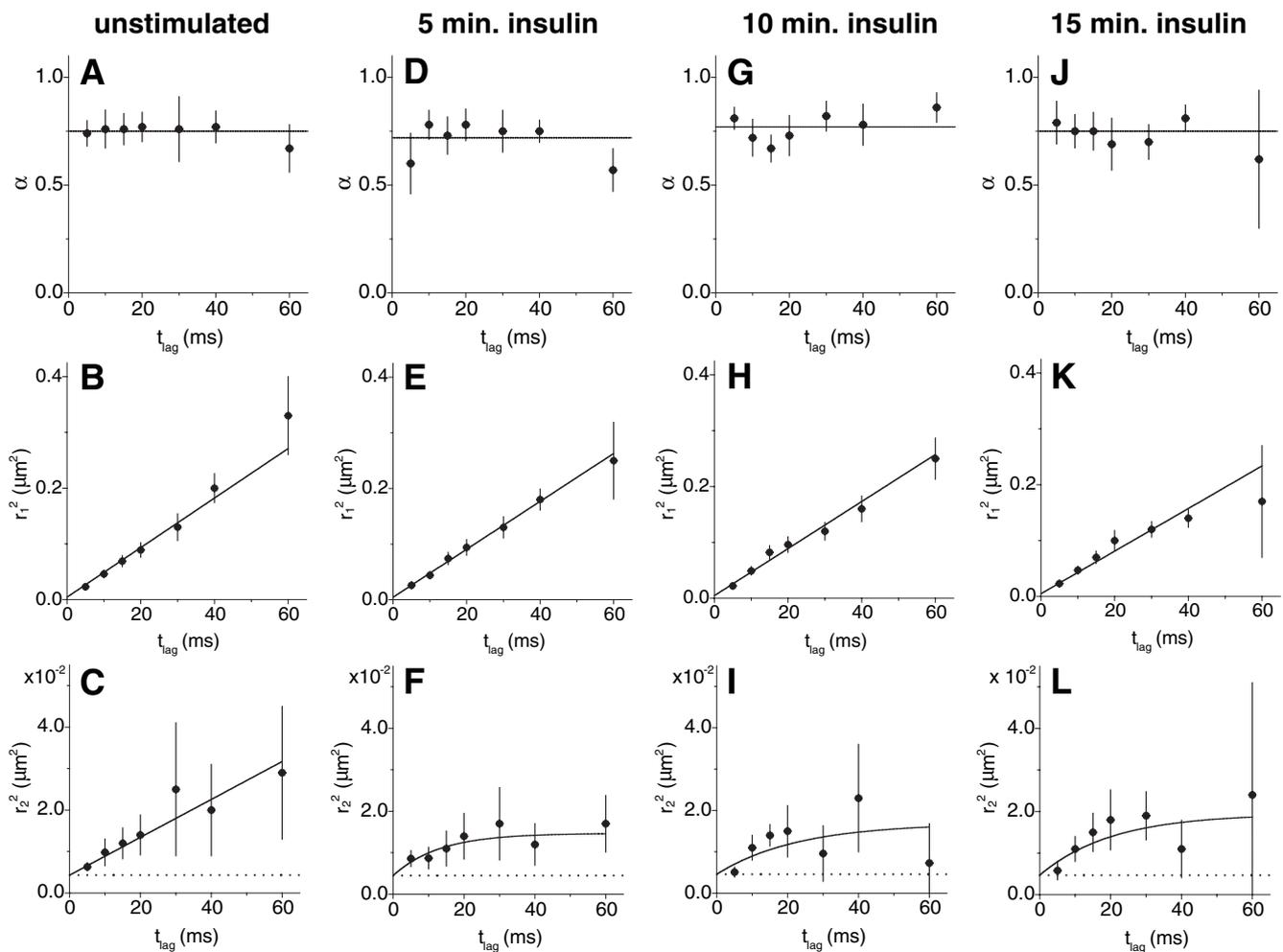

Fig. 5. Diffusion characteristics of eYFP-H-Ras(wt) before stimulation and 5, 10 and 15 minutes after stimulation with insulin. (A,D,G,J) Fast-diffusing fraction of molecules, α, versus timelag. The solid lines show the weighted mean of the fast fraction of molecules over all timelags. (B,E,H,K) Mean square displacement of the fast-diffusing fraction, r_1^2, plotted versus timelag. The data were fitted according to a free diffusion model ($r_1^2 = 4D_1 t_{lag}$, solid line). (C,F,I,L) Mean square displacement of the slow-diffusing fraction, r_2^2, plotted versus timelag. The data in C was fitted to a free diffusion model (solid line); the data in F,I,L were fitted according to a confined diffusion model (Eqn 3, solid line). The dotted lines in the plots of the bottom row represent the offset due to the limited positional accuracy (see Materials and Methods); although the same offset is present in the plots of the middle row, the dotted lines were omitted here for clarity.

immobile in the FRET study. Hence, the domain fraction in our study overlaps at least partially with the immobile fraction in the FRET study.

The reduction in the mobility of the mobile fraction of molecules observed in the FRET study, was also observed in our study, although to a lesser extent. The diffusion coefficient of the fast, free-diffusing fraction of H-Ras(V12) is 17% lower than the diffusion coefficient of H-Ras(N17) and 23% lower that the diffusion coefficient of GDP-loaded H-Ras(wt) (Table 1); relatively small decreases compared to the ~75% reduction observed on the 200 msecond timescale of the FRET study.

One possible explanation for the slight decrease in mobility of active H-Ras suggested in other studies is its transient binding to signaling complexes (Murakoshi et al., 2004) or small (40-50 nm) non-raft domains (Niv et al., 2002; Prior et al., 2003; Rotblat et al., 2004). At longer timelags such transient binding would slow down diffusion as described by an anomalous diffusion model (Saxton, 1996). Such a slow down of the diffusion at longer timelags was indeed observed: for H-Ras(wt) 15 minutes after insulin addition the r^2 values at longer timelags (40 and 60 milliseconds) were lower than predicted for a free diffusion model (Fig. 5K). A fit of the 15-minute activated H-Ras(wt) data and H-RasV12 data to an anomalous diffusion model, $r_1^2 \sim (t_{lag})^\gamma$, resulted in anomalous diffusion exponents, γ, of 0.89±0.08 for eYFP-H-Ras(V12) (Fig. 7A) and 0.81±0.12 for 15 minute-activated eYFP-H-Ras(wt) (Fig. 7B) respectively. When this last value is used to extrapolate the mean square displacement (MSD) of the fast fraction of 15 minute-activated H-Ras(wt) as observed in our study to the 200 mseconds timescale of the FRET study, an extrapolated MSD_{200ms} of 0.51 μm^2 is found. Although this extrapolation has to be treated with caution, it means a reduction of 43% compared to the extrapolated MSD_{200ms} before stimulation (0.89 μm^2), closer to, but still short of the 75% reduction observed in the FRET study (Murakoshi et al., 2004).

Comparison to FRAP and EM results of H-Ras activation and microdomain localization

It is interesting to compare our findings with the results of FRAP experiments, which cover a longer (~10 seconds) timescale (Niv et al., 2002). The latter showed that, at moderate expression level, the mobile fraction of GFP-H-Ras(V12) was about 20% slower than the mobile fraction of non-activated GFP-H-Ras(wt). As this difference was absent at higher expression levels and was not sensitive to cholesterol depletion, it was attributed to the association of active Ras with saturable nonraft sites. The immobile fraction of H-Ras was independent of the activation state and varied from 10-13%. Furthermore, it was shown that cholesterol depletion increased the diffusion coefficient of non-activated GFP-H-Ras(wt) by a factor of 2, indicating an association with lipid rafts.

The most pronounced difference between our single-molecule study and the FRAP results is that the fraction (39%) of H-Ras(V12) found in 200 nm domains in our study is significantly larger than the immobile fraction (10-13%) detected in the FRAP study. Assuming that the 200 nm domains are immobile and do not exchange Ras(V12) molecules with the free-diffusing population during a FRAP experiment (~10 seconds), they should give rise to an immobile fraction of the same size (~39%). The fact that the immobile fraction detected in the FRAP experiments was much lower (10-13%), indicates that H-Ras(V12) molecules are probably loosely associated with the observed 200 nm domains, in agreement with a model for dynamic association of activated H-Ras with nonraft sites (Niv et al., 2002). Furthermore, the relatively small decrease in diffusion coefficient of H-Ras(V12) compared with non-activated H-Ras(wt) found in the FRAP study, agrees well to the small difference in diffusion coefficient found for the fast, free-diffusing fraction of eYFP-H-Ras(V12) and non-activated eYFP-H-Ras(wt) (see Table 1) in our study.

Implications of this study for models of H-Ras microlocalization

The results of the FRAP study (Niv et al., 2002) agree very well with results of EM experiments (Prior et al., 2003). These showed that the membrane anchor of H-Ras localizes to cholesterol-dependent ~44 nm diameter domains that cover about 35% of the membrane surface. H-Ras(V12) localizes to
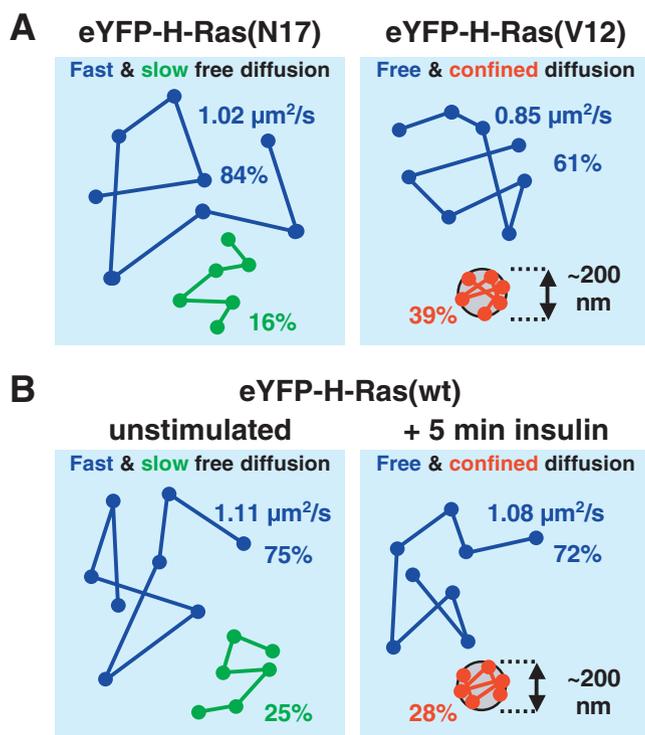

Fig. 6. (A) Schematic showing the differences in diffusion and domain localization between the inactive eYFP-H-Ras(N17) and active eYFP-H-Ras(V12) mutants. For both mutants the fast-diffusing fraction was freely diffusing (blue), but its size and diffusion coefficient were significantly smaller for the active H-Ras mutant than the inactive mutant. Also, the slow-diffusing fraction of the inactive mutant was freely diffusing (green), whereas it was confined in 200 nm domains for the active mutant (red). (B) Model depicting the effect of H-Ras(wt) activation on its diffusion characteristics. Before stimulation (left part) slow (25%, green) and fast (75%, blue) diffusing populations of H-Ras(wt) molecules were present, that were both freely diffusing. Activation of H-Ras(wt) by addition of insulin for 5 minutes resulted in the confinement of the slow-diffusing fraction in domains (red) with a diameter of ~200 nm.

A eYFP-H-Ras(V12)

B eYFP-H-Ras(wt)
15 min. insulin

Fig. 7. Mean square displacement of the fast fraction of the eYFP-H-Ras(V12) (A) and 15-minute stimulated eYFP-H-Ras(wt) (B) constructs. The dashed lines resulted from fits to the free diffusion model ($r_1^2 = 4D_1 t_{lag}$), the resulting diffusion coefficients (D_1) are given in Table 1. The solid lines represent fits to the anomalous diffusion model: $r_1^2 \sim (t_{lag})^\gamma$. The resulting anomalous diffusion exponents, γ, were 0.89 ± 0.08 for eYFP-H-Ras(V12) (A) and 0.81 ± 0.12 for 15 minute-activated eYFP-H-Ras(wt) (B), respectively.
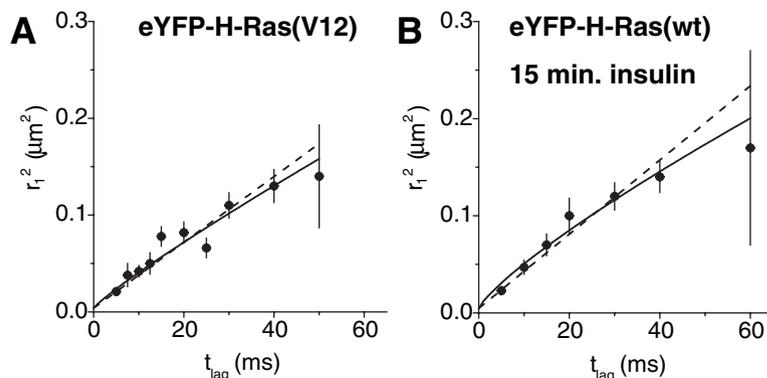
similar-sized domains that are not cholesterol, but galectin-1, dependent.

The results of our study are to a large extent in agreement with a recent model of H-Ras microlocalization and activation derived from the FRAP and EM experiments (Rotblat et al., 2004). Although the lipid-raft and non-raft domains in the Rotblat model (Rotblat et al., 2004) are too small (40-50 nm) to be directly observed by our technique, their presence would offer an explanation for the mobility changes of H-Ras observed in our study. The dynamic association of activated H-Ras with 40 nm non-raft domains as proposed by the model is in agreement with the relatively high diffusion coefficient of the fast-diffusing fraction of activated H-Ras observed in our study. Most probably the slow-diffusing fraction of activated H-Ras that is localized in 200 nm domains in our experiments results from a temporal trapping of the mobile 40 nm non-raft domains for at least 60 milliseconds. It is very likely that the actin cytoskeleton is involved in this temporal trapping, as insulin induces a rearrangement of the actin cytoskeleton (Li et al., 1993; Tsakiridis et al., 1998; Khayat et al., 2000; Dadke and Chernoff, 2003) and single-molecule FRET studies showed the involvement of actin in immobilization of active H-Ras (Murakoshi et al., 2004). A similar temporal trapping could also (partially) explain why 200 nm domains were observed in a previous diffusion study of the H-Ras membrane anchor (Lommerse et al., 2004), as this anchor is dynamically associated with small (40 nm diameter) lipid rafts according to the Rotblat model (Rotblat et al., 2004).

Furthermore it was proposed that the inactive wild-type H-Ras is in dynamic equilibrium between the lipid rafts and the non-raft domains (Rotblat et al., 2004). The large (75-84%) fast-diffusing fraction of inactive H-Ras, which has a slightly higher diffusion coefficient than the comparable fraction of activated Ras, is in agreement with the lack of 'stable' domain association in the model of Rotblat et al. However, the reason for the non-confined, slow-diffusing fraction of inactive H-Ras remains unclear. It could be caused by an unstable association with the 40 nm raft or non-raft domains or an association with Ras-binding molecules that slow-down the diffusion. One candidate is the GEF Son of Sevenless (SOS) for which a second, allosteric site that can bind either GTP-Ras or GDP-Ras has recently been discovered (Sondermann et al., 2004). Binding of SOS to a fraction of inactive eYFP-H-Ras could make inactive eYFP-H-Ras part of a small, slow-diffusing, molecular complex. Furthermore, the S17N mutation present in eYFP-H-Ras(N17) results in a reduced dissociation of

Ras(N17) from GEFs (Chen et al., 1994; Jung et al., 1994), potentially leading to GEF sequestering and complex formation.

In conclusion, the results of our short-timescale single-molecule study partially agree with the results of the FRET, FRAP and EM experiments. The high positional accuracy (35 nm) and temporal resolution (10-60 milliseconds) of our study enabled us to detect the partial localization of active H-Ras to 200 nm domains (Fig. 6). The localization of active Ras to these 200 nm domains is explained by a temporal trapping of mobile (40-50 nm) cholesterol-independent, domains (Rotblat et al., 2004) or transient signaling complexes (Murakoshi et al., 2004), with which active H-Ras dynamically associates. Most likely, the actin cytoskeleton meshwork is involved in this temporal trapping (Fujiwara et al., 2002; Ike et al., 2003). The observed 200 nm domains add another layer of organization to the H-Ras mobility-activation models, which could be applicable to other membrane-anchored signaling proteins, such as Src kinases.

References

Almeida, P. F. F. and Vaz, W. L. C. (1995). Lateral diffusion in membranes. In *Handbook of Biological Physics* (ed. R. Lipowsky and E. Sackmann), pp. 305-357. Amsterdam: Elsevier/North Holland.

Anderson, C. M., Georgiou, G. N., Morrison, I. E., Stevenson, G. V. and Cherry, R. J. (1992). Tracking of cell surface receptors by fluorescence digital imaging microscopy using a charge-coupled device camera. Low-density lipoprotein and influenza virus receptor mobility at 4 degrees C. *J. Cell Sci.* **101**, 415-425.

Apolloni, A., Prior, I. A., Lindsay, M., Parton, R. G. and Hancock, J. F. (2000). H-ras but not K-ras traffics to the plasma membrane through the exocytic pathway. *Mol. Cell. Biol.* **20**, 2475-2487.

Bernards, A. (2003). GAPs galore! A survey of putative Ras superfamily GTPase activating proteins in man and Drosophila. *Biochim. Biophys. Acta* **1603**, 47-82.

Bradford, M. M. (1976). A rapid and sensitive method for the quantitation of microgram quantities of protein utilizing the principle of protein-dye binding. *Anal. Biochem.* **72**, 248-254.

Brown, D. A. and Rose, J. K. (1992). Sorting of GPI-anchored proteins to glycolipid-enriched membrane subdomains during transport to the apical cell surface. *Cell* **68**, 533-544.

Burgering, B. M., Medema, R. H., Maassen, J. A., van de Wetering, M. L., van der Eb, A. J., McCormick, F. and Bos, J. L. (1991). Insulin stimulation of gene expression mediated by p21ras activation. *EMBO J.* **10**, 1103-1109.

Chen, S. Y., Huff, S. Y., Lai, C. C., Der, C. J. and Powers, S. (1994). Ras-15A protein shares highly similar dominant-negative biological properties with Ras-17N and forms a stable, guanine-nucleotide resistant complex with CDC25 exchange factor. *Oncogene* **9**, 2691-2698.

Choy, E., Chiu, V. K., Silletti, J., Feoktistov, M., Morimoto, T., Michaelson, D., Ivanov, I. E. and Philips, M. R. (1999). Endomembrane trafficking of ras: the CAAX motif targets proteins to the ER and Golgi. *Cell* **98**, 69-80.

Cowley, S., Paterson, H., Kemp, P. and Marshall, C. J. (1994). Activation of MAP kinase kinase is necessary and sufficient for PC12 differentiation and for transformation of NIH 3T3 cells. *Cell* **77**, 841-852.

Dadke, S. and Chernoff, J. (2003). Protein-tyrosine phosphatase 1B mediates the effects of insulin on the actin cytoskeleton in immortalized fibroblasts. *J. Biol. Chem.* **278**, 40607-40611.

Ehrhardt, A., Ehrhardt, G. R., Guo, X. and Schrader, J. W. (2002). Ras and relatives – job sharing and networking keep an old family together. *Exp. Hematol.* **30**, 1089-1106.

Elad-Sfadia, G., Haklai, R., Ballan, E., Gabius, H. J. and Kloog, Y. (2002). Galectin-1 augments Ras activation and diverts Ras signals to Raf-1 at the expense of phosphoinositide 3-kinase. *J. Biol. Chem.* **277**, 37169-37175.

Farnsworth, C. L. and Feig, L. A. (1991). Dominant inhibitory mutations in the Mg(2+)-binding site of RasH prevent its activation by GTP. *Mol. Cell. Biol.* **11**, 4822-4829.

Feig, L. A. and Cooper, G. M. (1988). Inhibition of NIH 3T3 cell proliferation by a mutant ras protein with preferential affinity for GDP. *Mol. Cell. Biol.* **8**, 3235-3243.

Fujiwara, T., Ritchie, K., Murakoshi, H., Jacobson, K. and Kusumi, A. (2002). Phospholipids undergo hop diffusion in compartmentalized cell membrane. *J. Cell Biol.* **157**, 1071-1081.

Hancock, J. F., Paterson, H. and Marshall, C. J. (1990). A polybasic domain or palmitoylation is required in addition to the CAAX motif to localize p21ras to the plasma membrane. *Cell* **63**, 133-139.

Hancock, J. F., Cadwallader, K., Paterson, H. and Marshall, C. J. (1991). A CAAX or a CAAL motif and a second signal are sufficient for plasma membrane targeting of ras proteins. *EMBO J.* **10**, 4033-4039.

Harms, G. S., Cognet, L., Lommerse, P. H. M., Blab, G. A. and Schmidt, T. (2001). Autofluorescent proteins in single-molecule research: applications to live cell imaging microscopy. *Biophys. J.* **80**, 2396-2408.

Ike, H., Kosugi, A., Kato, A., Iino, R., Hirano, H., Fujiwara, T., Ritchie, K. and Kusumi, A. (2003). Mechanism of Lck recruitment to the T-cell receptor cluster as studied by single-molecule-fluorescence video imaging. *Chem. Phys. Chem.* **4**, 620-626.

Jung, V., Wei, W., Ballester, R., Camonis, J., Mi, S., van Aelst, L., Wigler, M. and Broek, D. (1994). Two types of RAS mutants that dominantly interfere with activators of RAS. *Mol. Cell. Biol.* **14**, 3707-3718.

Khayat, Z. A., Tong, P., Yaworsky, K., Bloch, R. J. and Klip, A. (2000). Insulin-induced actin filament remodeling colocalizes actin with phosphatidylinositol 3-kinase and GLUT4 in L6 myotubes. *J. Cell Sci.* **113**, 279-290.

Kusumi, A., Sako, Y. and Yamamoto, M. (1993). Confined lateral diffusion of membrane receptors as studied by single particle tracking (nanovid microscopy). Effects of calcium-induced differentiation in cultured epithelial cells. *Biophys. J.* **65**, 2021-2040.

Li, S. L., Miyata, Y., Yahara, I. and Fujita-Yamaguchi, Y. (1993). Insulin-induced circular membrane ruffling on rat 1 cells expressing a high number of human insulin receptors: circular ruffles caused by rapid actin reorganization exhibit high density of insulin receptors and phosphotyrosines. *Exp. Cell Res.* **205**, 353-360.

Lommerse, P. H. M., Blab, G. A., Cognet, L., Harms, G. S., Snaar-Jagalska, B. E., Spaink, H. P. and Schmidt, T. (2004). Single-molecule imaging of the H-Ras membrane-anchor reveals domains in the cytoplasmic leaflet of the cell membrane. *Biophys. J.* **86**, 609-616.

Murakoshi, H., Iino, R., Kobayashi, T., Fujiwara, T., Ohshima, C., Yoshimura, A. and Kusumi, A. (2004). Single-molecule imaging analysis

of Ras activation in living cells. *Proc. Natl. Acad. Sci. USA* **101**, 7317-7322.

Niv, H., Gutman, O., Kloog, Y. and Henis, Y. I. (2002). Activated K-Ras and H-Ras display different interactions with saturable nonraft sites at the surface of live cells. *J. Cell Biol.* **157**, 865-872.

Parmryd, I., Adler, J., Patel, R. and Magee, A. I. (2003). Imaging metabolism of phosphatidylinositol 4,5-bisphosphate in T-cell GM1-enriched domains containing Ras proteins. *Exp. Cell Res.* **285**, 27-38.

Payne, D. M., Rossomando, A. J., Martino, P., Erickson, A. K., Her, J. H., Shabanowitz, J., Hunt, D. F., Weber, M. J. and Sturgill, T. W. (1991). Identification of the regulatory phosphorylation sites in pp42/mitogen-activated protein kinase (MAP kinase). *EMBO J.* **10**, 885-892.

Prior, I. A., Harding, A., Yan, J., Sluimer, J., Parton, R. G. and Hancock, J. F. (2001). GTP-dependent segregation of H-ras from lipid rafts is required for biological activity. *Nat. Cell Biol.* **3**, 368-375.

Prior, I. A., Muncke, C., Parton, R. G. and Hancock, J. F. (2003). Direct visualization of Ras proteins in spatially distinct cell surface microdomains. *J. Cell Biol.* **160**, 165-170.

Quilliam, L. A., Rebhun, J. F. and Castro, A. F. (2002). A growing family of guanine nucleotide exchange factors is responsible for activation of Ras-family GTPases. *Prog. Nucleic Acid Res. Mol. Biol.* **71**, 391-444.

Rotblat, B., Prior, I. A., Muncke, C., Parton, R. G., Kloog, Y., Henis, Y. I. and Hancock, J. F. (2004). Three separable domains regulate GTP-dependent association of H-ras with the plasma membrane. *Mol. Cell. Biol.* **24**, 6799-6810.

Saxton, M. J. (1996). Anomalous diffusion due to binding: a Monte Carlo study. *Biophys. J.* **70**, 1250-1262.

Schmidt, T., Schütz, G. J., Baumgartner, W., Gruber, H. J. and Schindler, H. (1995). Characterization of photophysics and mobility of single molecules in a fluid lipid membrane. *J. Phys. Chem.* **99**, 17662-17668.

Schmidt, T., Schütz, G. J., Baumgartner, W., Gruber, H. J. and Schindler, H. (1996). Imaging of single molecule diffusion. *Proc. Natl. Acad. Sci. USA* **93**, 2926-2929.

Schütz, G. J., Schindler, H. and Schmidt, T. (1997). Single-molecule microscopy on model membranes reveals anomalous diffusion. *Biophys. J.* **73**, 1073-1080.

Seeburg, P. H., Colby, W. W., Capon, D. J., Goedel, D. V. and Levinson, A. D. (1984). Biological properties of human c-Ha-ras1 genes mutated at codon 12. *Nature* **312**, 71-75.

Simons, K. and Ikonen, E. (1997). Functional rafts in cell membranes. *Nature* **387**, 569-572.

Sondermann, H., Soisson, S. M., Boykevisch, S., Yang, S. S., Bar-Sagi, D. and Kuriyan, J. (2004). Structural analysis of autoinhibition in the Ras activator Son of sevenless. *Cell* **119**, 393-405.

Sturgill, T. W., Ray, L. B., Erikson, E. and Maller, J. L. (1988). Insulin-stimulated MAP-2 kinase phosphorylates and activates ribosomal protein S6 kinase II. *Nature* **334**, 715-718.

Suire, S., Hawkins, P. and Stephens, L. (2002). Activation of phosphoinositide 3-kinase gamma by Ras. *Curr. Biol.* **12**, 1068-1075.

Tsakiridis, T., Bergman, A., Somwar, R., Taha, C., Aktories, K., Cruz, T. F., Klip, A. and Downey, G. P. (1998). Actin filaments facilitate insulin activation of the src and collagen homologous/mitogen-activated protein kinase pathway leading to DNA synthesis and c-fos expression. *J. Biol. Chem.* **273**, 28322-28331.

van Deurs, B., Roepstorff, K., Hommelgaard, A. M. and Sandvig, K. (2003). Caveolae: anchored, multifunctional platforms in the lipid ocean. *Trends Cell Biol.* **13**, 92-100.

van Meer, G. and Simons, K. (1988). Lipid polarity and sorting in epithelial cells. *J. Cell Biochem.* **36**, 51-58.

Voice, J. K., Klemke, R. L., Le, A. and Jackson, J. H. (1999). Four human ras homologs differ in their abilities to activate Raf-1, induce transformation, and stimulate cell motility. *J. Biol. Chem.* **274**, 17164-17170.

Willumsen, B. M., Christensen, A., Hubbert, N. L., Papageorge, A. G. and Lowy, D. R. (1984). The p21 ras C-terminus is required for transformation and membrane association. *Nature* **310**, 583-586.

Yan, J., Roy, S., Apolloni, A., Lane, A. and Hancock, J. F. (1998). Ras isoforms vary in their ability to activate Raf-1 and phosphoinositide 3-kinase. *J. Biol. Chem.* **273**, 24052-24056.

Zacharias, D. A., Violin, J. D., Newton, A. C. and Tsien, R. Y. (2002). Partitioning of lipid-modified monomeric GFPs into membrane microdomains of live cells. *Science* **296**, 913-916.